An Alternative Approach for the Incorporation of Cellulose Nanocrystals in Flexible Polyurethane Foams Based On Renewably Sourced Polyols

(http://dx.doi.org/10.1016/j.indcrop.2016.11.011)

Lorena Ugarte [a], Arantzazu Santamaría-Echart [a], Stefan Mastel [b], Marta Autore [b], Rainer Hillenbrand [c,d], Maria Angeles Corcuera [a], Arantxa Eceiza [a,]*

[a] Materials + Technologies Research Group (GMT), Department of Chemical and Environmental Engineering, Faculty of Engineering of Gipuzkoa, University of the Basque Country (UPV/EHU), 20018 Donostia-San Sebastian, Spain. * arantxa.eceiza@ehu.eus

[b] CIC NanoGUNE, E-20018, Donostia-San Sebastián, Spain

[c] CIC NanoGUNE and UPV/EHU, E-20018, Donostia-San Sebastian, Spain

[d] IKERBASQUE, Basque Foundation for Science, 48011, Bilbao, Spain

KEYWORDS: cellulose nanocrystals, renewable polyols, polyurethane foam nanocomposites, mechanical properties, nano/microstructure, nanospectroscopy

Abstract

This work analyzes not only the effect of cellulose nanocrystals on final properties of castor oil and corn based flexible polyurethane foam nanocomposites but also a deep analysis about the changes on micro/nanostructure and morphology is carried out. Cellulose nanocrystals were isolated from microcrystalline cellulose by acid hydrolysis and incorporated in aqueous suspension to renewably sourced polyols for foam synthesis. The effect of cellulose nanocrystals percentage on cell morphology, nano/microstructure and properties of the foam nanocomposites was analyzed by scanning electron microscopy, atomic force microscopy, Fourier transform infrared spectroscopy, compressive mechanical properties, hysteresis and resilience tests and dynamic mechanical analysis. To verify the presence of cellulose

nanocrystals in the foam cell walls, infrared near-field microscopy and nanospectroscopy were employed. Results suggested that interactions between cellulose nanocrystals and polyurethane hard segments occurred and foam cell walls were reinforced. The overall reinforcing effect showed to be dependent on the cellular structure of the foam, which was in turn influenced by the presence of cellulose nanocrystals.

1. INTRODUCTION

The increase of global environmental awareness and the depletion of fossil resources have promoted the use of renewably sourced polymers and raw materials for polymer synthesis (Williams and Hillmyer, 2016). For example, vegetable oils such as castor oil or soybean oil have shown great potential to be used as polyols in polyurethane synthesis (Petrovic, 2008; Zhang et al., 2015) and this way reduce the amount of petrochemical precursors in the final material. In the nanocomposites field, cellulose, the most common biopolymer on earth, (Klemm et al., 2005) has become an interesting source of nanoreinforcements in the form of cellulose nanofibers (CNF) or cellulose nanocrystals (CNCs) which are characterized by their low density, high modulus and tensile strength, biodegradability, renewability and availability (Mariano et al., 2014). Apart from their renewable nature, nanoreinforcements are known to enhance mechanical properties of the matrix at low levels of filler content, (Mittal, 2010) resulting in lower environmental impact. Although wood is the main cellulosic source, annual plants as well as agroforestry or industrial residues have great potential as sources of cellulosic nanomaterials (Jonoobi et al., 2015). CNCs have been widely used in polyurethane nanocomposites due to the aforementioned superior mechanical properties and environmental advantages. The common methods for the synthesis of polyurethane nanocomposites include solvent casting (De Oliveira Patricio et al., 2013; Rueda et al., 2013b), melt blending (Ramôa et al., 2013; Valentini et al., 2015) and in-situ polymerization

(Rueda et al., 2013a; Saralegi et al., 2014). In the case of polyurethane foams, which present a crosslinked structure, the solvent casting and melt blending procedures are not suitable and hence the in-situ polymerization technique is used adding the nanoreinforcement to the polyurethane precursors at the beginning of the polymerization (Alavi Nikje et al., 2014; Bernal et al., 2011). One of the main challenges in the incorporation of the nanoreinforcements is to obtain a good dispersion of nanoentities so that a close interaction is created between the matrix and the nanoreinforcement and mechanical properties are enhanced (Hussain et al., 2006). In works concerning flexible polyurethane foam/CNC nanocomposites, the nanoentities were incorporated to the polyol component in solid state. Mosiewicki et al. (Mosiewicki et al., 2015) incorporated commercial micro/nano cellulose directly to the polyol and mixed by mechanical stirring. Cordero et al. (Cordero et al., 2015) dehydrated a CNC suspension obtained by acid hydrolysis and mixed with the polyol by sonication. It is accepted that the sulfate groups at the CNC surface introduced by sulfuric acid hydrolysis cause electrostatic repulsion between particles resulting in stable aqueous suspensions (Beck et al., 2012). However, when CNCs are dried, agglomerates could be formed depending on the drying technique and their redispersibility even in water is compromised due to strong hydrogen bonding generated in the cellulose backbone (Dong and Gray, 1997; Khoshkava and Kamal, 2014). One alternative of redispersion consists on the use of polar organic solvents and its subsequent removal, but the redispersion seems not to be complete even this way (Viet et al., 2007).

In this work the effect of CNCs not only on the final properties of the foam nanocomposites but also on the morphology and micro/nanostructure of the nanocomposites was analyzed since the effect on final properties is a consequence of the changes in morphology and

micro/nanostructure caused by the incorporation of nanoentities. CNCs were isolated by acid hydrolysis from microcrystalline cellulose (MCC) and their sulfur content and morphology were characterized by elemental analysis, conductometric titration and atomic force microscopy (AFM). The aqueous CNCs dispersion obtained after CNCs isolation procedure was directly incorporated in a renewably sourced polyol mixture. This way, CNCs drying and redispersion steps or the use of pollutant organic solvents were avoided. After removing the water from the polyol-CNCs mixture, foams were synthesized in a one shot method in open molds. To analyze the effect of different CNC percentages on the morphology, microstructure and final properties of the foam nanocomposites scanning electron microscopy (SEM), Fourier transform infrared (FTIR) spectroscopy, compressive mechanical tests, resilience test, dynamical mechanic analysis (DMA), AFM and infrared near-field microscopy (IR s-SNOM) and nanospectroscopy (nano-FTIR) were used.

Because s-SNOM and nanoFTIR are relatively new techniques, in the following their basic working principles are briefly described.

IR s-SNOM and nano-FTIR spectroscopy (Huth et al., 2012, 2011; Keilmann and Hillenbrand, 2009) allow for infrared imaging and spectroscopy with nanoscale spatial resolution. s-SNOM is based on an AFM employing a metalized tip, which is illuminated with monochromatic infrared laser radiation. The tip acts as an antenna and concentrates the infrared field at the tip apex. Due to near-field interaction of this strongly localized field with the sample surface, the tip-scattered field contains information about the infrared sample properties. Interferometric detection of the tip-scattered light - simultaneously to the AFM topography - yields nanoscale resolved infrared amplitude and phase infrared images, providing maps of the chemical properties of the sample surface. Nano-FTIR is based on s-

SNOM. The tip is illuminated with a broadband infrared radiation. At a fixed sample position, the tip-scattered light is recorded with an asymmetric Fourier transform spectrometer, yielding amplitude- and phase-resolved infrared spectra.

The spatial resolution of s-SNOM and nano-FTIR only depends on the tip diameter, which is typically in the order of a few ten nanometers for commonly used commercial tips (Govyadinov et al., 2014). It is thus improved by more than a factor of 100 compared to standard FTIR spectroscopy.

In this work s-SNOM phase images and nano-FTIR phase spectra are shown, revealing information about the infrared absorption and thus chemical composition of the sample (Govyadinov et al., 2014, 2013; Huth et al., 2012; Mastel et al., 2015).

2. EXPERIMENTAL

2.1. Raw materials

Castor oil based Lupranol Balance 50® (P1) (BASF, 49.7 mg KOH/g, 1129 g/eq) and corn sugar based polytrimethylene ether glycol (P2) (79.4 mg KOH/g, 706 g/eq) were used as polyol components. Amine catalyst Tegoamin® B75, tin catalyst Kosmos® 29 and surfactant Tegostab® B-4900 were supplied by Evonik. Toluene diisocyanate (TDI), generously supplied by Bayer was used with a constant isocyanate index of 120. Distilled water was used as blowing agent. Microcrystalline cellulose (MCC) and sulfuric acid (H_2SO_4) (96%) were supplied from Aldrich.

2.2. Isolation of cellulose nanocrystals

MCC was subjected to sulfuric acid hydrolysis to remove the amorphous regions (Rueda et al., 2013a; Saralegi et al., 2014). MCC was mixed with H_2SO_4 (64%) at 45 ºC for 30 min. Deionized water was added to stop the hydrolysis process. The diluted suspensions were centrifuged at 4000 rpm for 20 min and the CNC rich sediment was collected. Finally, pH was stabilized at 5-6 value by a dialysis process against deionized water. An aqueous suspension of 0.5 wt % CNC was obtained.

2.3. Synthesis of foam nanocomposites

Foams were synthesized in a one shot method as previously reported (Ugarte et al., 2014). Prior to the foaming process, the CNC suspension was incorporated to the polyol component as follows. The CNC suspension was first sonicated in an ultrasonic bath for 30 min and thereafter incorporated to the polyol. Water was removed by vacuum while the mixture was continuously stirred. Water elimination was checked by weight difference and thermogravimetric analysis (TGA). The resulting polyol-CNC dry mixture was first sonicated for 30 min and then mixed at high speed for 10 min with a high shear stirrer. For foaming, water, catalysts and surfactant were incorporated and mixed with the polyol-CNC dry mixture for 90 s at 2000 rpm. Water, catalysts and surfactant quantities were maintained constant at 3.5, 0.7 and 1.1 parts per hundred polyol (pphp), respectively. Finally, TDI was incorporated and mixed for 10 s. The resulting foam nanocomposites were left to rise freely and cured for 24 h before demolding. The designation and formulation of foam nanocomposites are summarized in Table 1. For comparative purposes, polyurethane foam matrixes were also synthesized.

Table 1. Designation and formulation of polyurethane neat foams and foam nanocomposites.

Sample	P1 (pphp)	P2 (pphp)	TDI (g)	CNC (wt %)
PF100	100	-	49.3	-
PF100-0.5	100	-	49.3	0.5
PF100-0.75	100	-	49.3	0.75
PF100-1.5	100	-	49.3	1.5
PF80	80	20	50.6	-
PF80-0.75	80	20	50.6	0.75
PF80-1.5	80	20	50.6	1.5

2.4. Characterization

2.4.1. Determination of sulfur content in CNCs

The sulfur content in CNCs introduced by sulfuric acid hydrolysis was determined by conductometric titration carried out at room temperature using a Crison EC-Meter GLP 31 instrument calibrated with 147 μS cm^{-1}, 1413 μS cm^{-1} and 12.88 mS cm^{-1} standards. NaOH and HCl 10 mM were used for the titration. Elemental analysis was also carried out for sulfur content determination using a Euro EA3000 Elemental Analyzer (Eurovector).

2.4.2. Atomic force microscopy (AFM)

AFM technique was used to observe the morphology of CNCs and foam nanocomposites. For CNCs sample preparation, a droplet of diluted CNC suspension was placed in a mica substrate and spin coated at 2000 rpm for 120 s. For foam nanocomposites sample preparation

epoxy filling technique and posterior cryo-ultramicrotomy were used. This technique is useful for the analysis of the nano/microstructure of polyurethane foams since the epoxy does not alter the foam morphology (Lan and Haugstad, 2011). For that, small foam pieces were embedded with epoxy to fill the foam pores and the air entrapped was removed by applying low vacuum. The epoxy was cured at 60 ºC for 24 h and the resulting specimens were cut with a Leica EM FC6 cryo-ultramicrotome equipped with a diamond knife and operated at -120 ºC. AFM images of foam cell struts were obtained in tapping mode at room temperature with a Nanoscope IIIa scanning probe microscope (Multimode^{TM}, Digital Instruments), using an integrated force generated by cantilever/silicon probes, applying a resonance frequency of ca 180 kHz. The cantilevers were 125 nm long, with a tip radius of 5-10 nm. The AFM tip was positioned over the foam cell struts to observe their morphology (Ugarte et al., 2014).

2.4.3. Thermogravimetric analysis (TGA)

TGA was performed on a TGA/SDTA 851 Mettler Toledo equipment to follow the drying process of polyol-CNC mixture. Samples were heated from room temperature to 650 ºC at a heating rate of 10 ºC min^{-1} under a nitrogen atmosphere. Samples were considered dry when no peak assigned to water evaporation was observed at around 100 ºC.

2.4.4. Density and cell morphology

Cell morphology was analyzed by scanning electron microscopy (SEM) technique using a JEOL-JSM-6400 equipment operated at 20kV and beam currents between 0.01 and 0.1 nA. Prior to analysis, the samples were gold coated. Images both in perpendicular and parallel directions to cell growth were obtained. For determining the cell dimensions, an average of 15 measurements were performed both in perpendicular and parallel direction images,

measuring the longitudinal length (L) and transversal width (T) dimensions for each cell. Core density of bare foams and foam nanocomposites was determined according to ASTM D-3574-11 standard.

2.4.5. Attenuated total reflectance Fourier transform infrared spectroscopy (ATR-FTIR)

ATR-FTIR spectroscopy was used to identify the characteristic functional groups of foam nanocomposites and CNCs. Measurements were performed with a Nicolet Nexus FTIR spectrometer equipped with a MKII Golden Gate accessory, Specac, with diamond crystal as ATR element at a nominal incidence angle of 45º with a ZnSe lens. Single-beam spectra of the samples were obtained after averaging 64 scans in the range from 4000 to 800 cm^{-1} with a resolution of 4 cm^{-1}.

2.4.6. Mechanical properties

Mechanical properties of foam nanocomposites were evaluated in a MTS equipment with a load cell of 250 N. Compressive tests were carried out using rectangular samples of 20 mm x 20 mm x 10 mm (length x width x thickness). One compression cycle was performed for each sample at a crosshead speed of 50 mm min^{-1} compressing the foam nanocomposites until 75% strain and posterior unloading. The compressive force was applied in the foam rise direction. The compressive modulus and the compressive strength, defined as the stress at 10% strain, were measured. Hysteresis loss was calculated according to ASTM D3574-11 standard, measuring the areas under the stress strain curve in the compression and decompression cycles. Resilience of foam nanocomposites was calculated using a Bareiss® Ball Rebound Tester, according to ASTM D3574-11 standard, test H. All properties were averaged from at least three specimens.

2.4.7. Dynamic mechanical analysis (DMA)

DMA was performed in tensile mode by an Eplexor 100N analyzer, Gabo equipment. Measurements were carried out at a scanning rate of 2 ºC min^{-1} from -100 ºC to 200 ºC with an initial strain of 2% and operating at 1 Hz frequency. Samples of 20 mm x 5.5 mm x 3.5 mm (length x width x thickness) were used.

2.4.8. Scattering-type scanning near-field infrared near-field microscopy (IR s-SNOM) and nanoscale-resolved Fourier transform infrared (nano-FTIR) spectroscopy

The IR s-SNOM images and nano-FTIR spectra, as well as the corresponding AFM images, were recorded with a neaSNOM system (Neaspec GmbH, Germany) comprising both s-SNOM and nano-FTIR capabilities. Pt-Si coated AFM tips were used. IR s-SNOM imaging of the foam cross sections were performed with illumination from a grating-tunable CO_2 laser. Nano-FTIR spectroscopy of a pure CNC sample was performed with illumination from a mid-infrared laser supercontinuum, using Au coated AFM tips. The final nano-FTIR spectra were obtained by averaging 25 individual spectra. The total acquisition time was 15 min and the spectral resolution 16 cm^{-1}. The spectra were normalized to that obtained on a clean gold surface (reference measurements).

3. RESULTS AND DISCUSSION

3.1. Cellulose nanocrystals

3.1.1. Morphology

Nanoentities of rod like shape were observed in CNC height images obtained by AFM (Figure 1 left), proving the efficacy of acid hydrolysis to isolate nanocrystals. Aspect ratio of

isolated CNCs was calculated performing 100 measurements. The length of CNCs was calculated from height images while height profiles were used for diameter estimation to avoid tip radius effects (Kvien et al., 2005). Average length value of 167 ± 31 nm and diameter value of 5.4 ± 1.5 were obtained, thus yielding an aspect ratio (L/D) of 31. An example of height profile measured along the white line is shown in Figure 1 right.

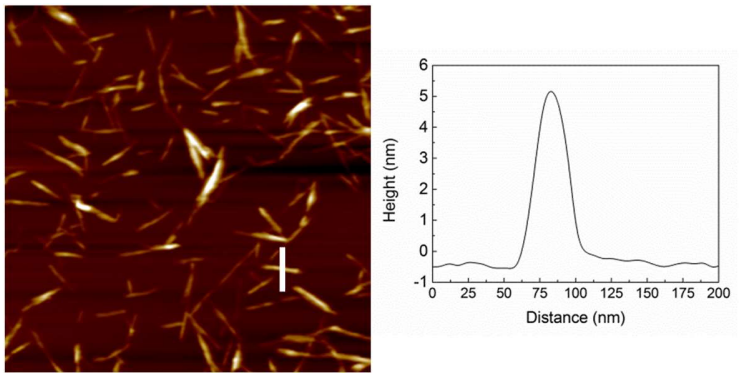

Figure 1. (left) AFM height image (size 2 x 2 μm) and (right) cross sectional height profile calculated along the white line.

3.1.2. Sulfur content

The sulfate group content on the surface of CNCs was calculated with conductometric titration (Dong et al., 1998; Espinosa et al., 2013), obtaining a sulfur content of 1.22%. In order to corroborate this result, elemental analysis of CNCs was performed which indicated a sulfur content of 1.28%. Results confirmed the anchoring of sulfate groups on the surface of CNCs.

3.1.3. Polyol/CNC mixture drying

Water reacts with isocyanate to yield urea and carbon dioxide which acts as foaming agent. In order to control the added water content and keep it constant in all formulations it was

necessary to dry the polyol/CNC mixtures prior to foaming. The drying process of polyol/CNC mixture was followed by weight difference and corroborated by TGA. The polyol/CNC mixture was considered free of water when no sign of water evaporation peak was observed in TGA thermogram. An example of polyol/CNC mixture drying TGA curve is shown in Figure 2.

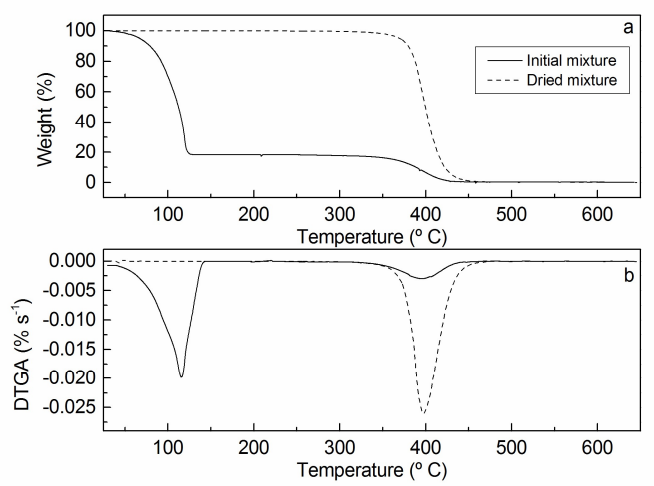

Figure 2. TGA and DTGA curves of initial (solid line) and dried (dashed line) polyol mixture for PF100-0.5 sample.

3.2. Foam nanocomposites

3.2.1. Morphology of the foams

SEM images of foams both in perpendicular and parallel directions to cell growth together with cell size distribution in longitudinal and transversal directions are shown in Figure 3 and Figure 4, respectively. Concerning the perpendicular direction (Figure 3), CNC incorporation caused an increase in cell heterogeneity in PF100 series due to the presence of big cells as it is observed on the broadening of cell size distribution. Although some big cells were also

observed in PF80 series, the effect was not so pronounced as in PF100 series and they showed more homogeneous morphology. Regarding the parallel direction (Figure 4), the anisotropy of cells seemed to increase with CNCs incorporation especially in PF80 series with increasing differences in cell size in longitudinal and transversal directions.

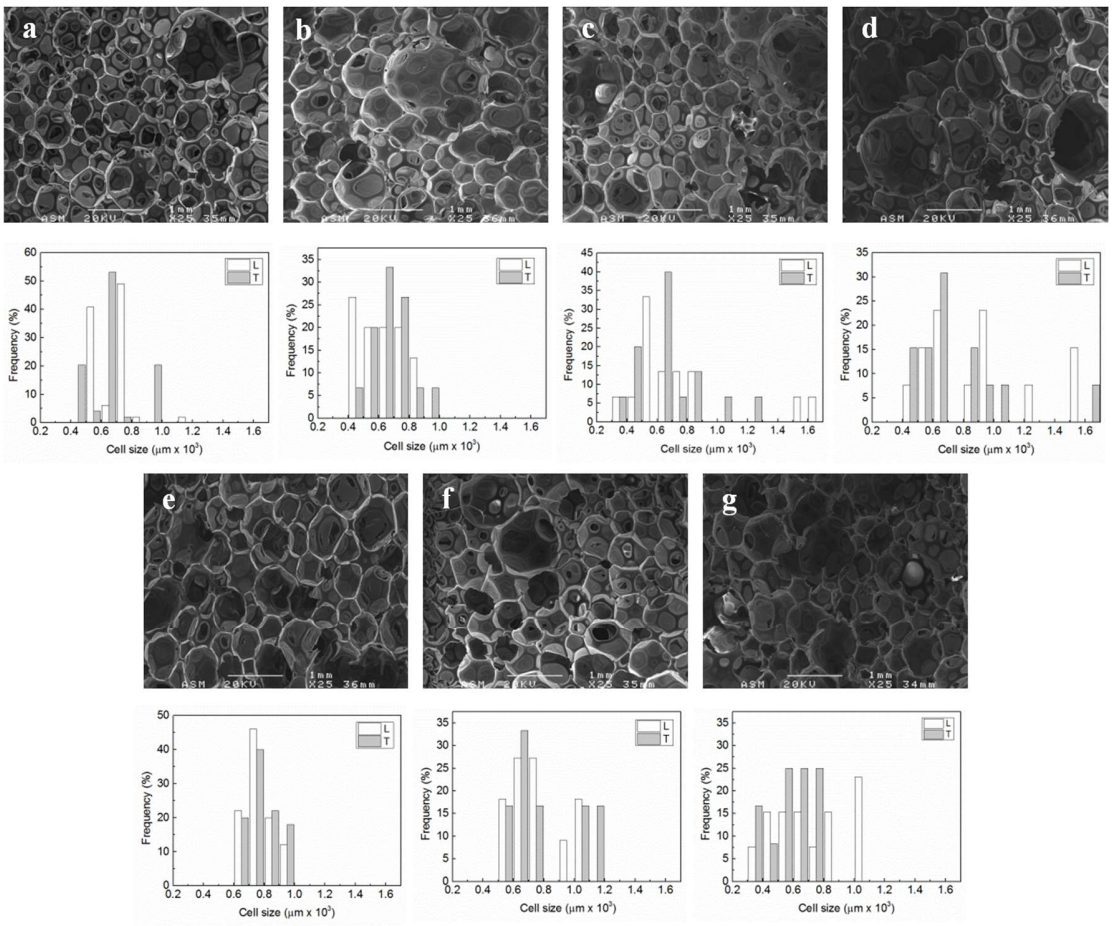

Figure 3. SEM images (X25) and the corresponding cell size distribution in the longitudinal (L) and transversal (T) directions of (a) PF100, (b) PF100-0.5, (c) PF100-0.75, (d) PF100-1.5, (e) PF80, (f) PF80-0.75 and (g) PF80-1.5 in the perpendicular direction to foam growth

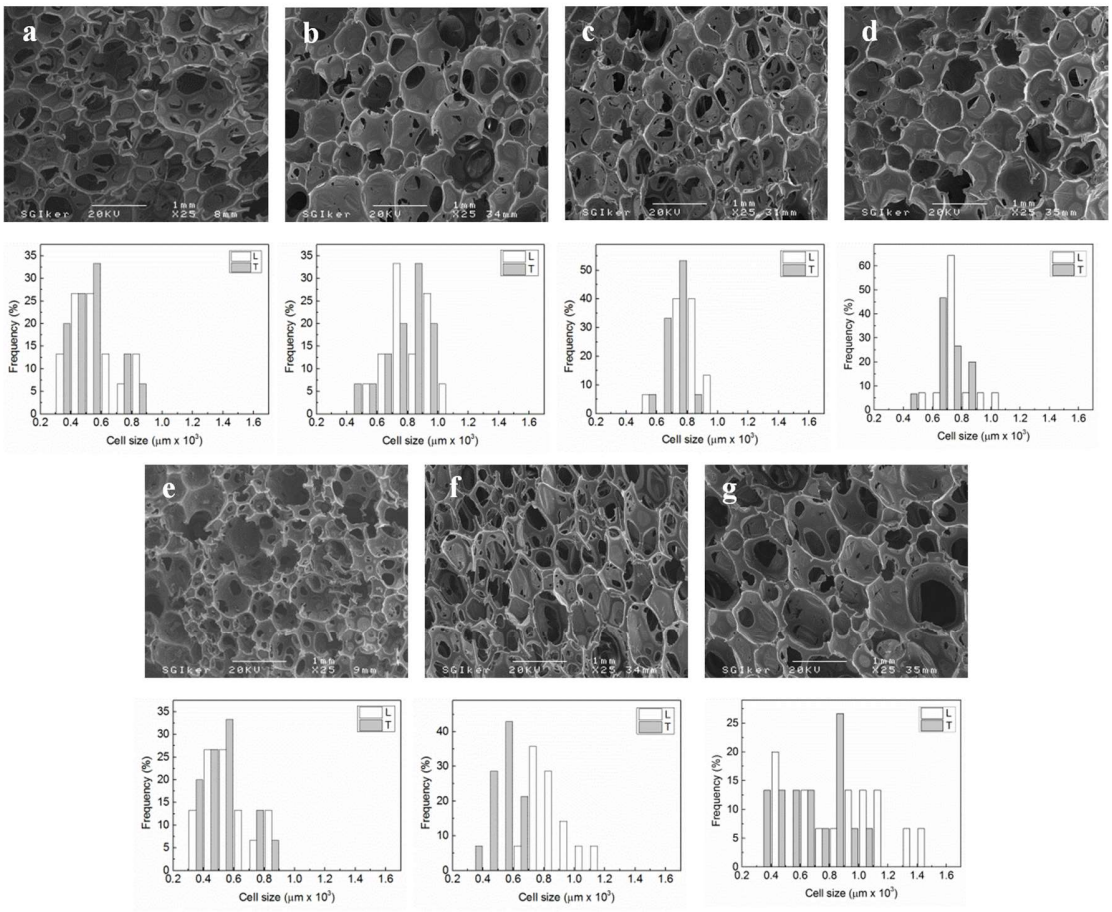

Figure 4. SEM images (X25) and the corresponding cell size distribution in the longitudinal (L) and transversal (T) directions of (a) PF100, (b) PF100-0.5, (c) PF100-0.75, (d) PF100-1.5, (e) PF80, (f) PF80-0.75 and (g) PF80-1.5 in the parallel direction to foam growth

As it is concluded from Figure 3 and Figure 4, the incorporation of CNCs influenced the foam morphology by increasing cell size, probably due to their effect in the mechanisms concerning the formation of the cellular structure. In particular, observing the increase in cell dimensions, it could be supposed that CNCs acted as particulate surfactants in spite of nucleating agents (Cordero et al., 2015; Malewska et al., 2015). Apart from the effect of CNCs, the incorporation of P2 polyol may also have affected the formation of cellular

structure due to its higher reactivity because of the primary hydroxyl groups and higher hydroxyl number (Ugarte et al., 2015, 2014).

For each sample, an approximated cell volume was calculated parting from the average cell radius, calculated from cell dimensions in longitudinal and transversal directions for both perpendicular and parallel SEM images. Although foam density is not only dependent on cell size but also on cell density and wall and/or strut thickness, results seemed to be in good agreement with density values shown in Table 2.

Table 2. Estimated average cell radius (r_{cell}) and cell volume (V_{cell}) of bare PU foams and foam nanocomposites

Sample	$r_{cell\ (\mu m)}$	V_{cell} (mm^3)	ρ (kg m^{-3})
PF100	304.81 ± 54.13	0.119 ± 6.6E-04	42.00 ± 0.97
PF100-0.5	360.32 ± 39.45	0.196 ± 2.6E-04	41.18 ± 0.21
PF100-0.75	369.03 ± 25.20	0.211 ± 6.7E-05	38.56 ± 1.23
PF100-1.5	389.05 ± 37.46	0.247 ± 2.2E-04	33.90 ± 0.98
PF80	303.16 ± 52.23	0.117 ± 6.0E-04	42.35 ± 0.94
PF80-0.75	370.69 ± 75.42	0.214 ± 1.8E-03	34.25 ± 0.59
PF80-1.5	358.30 ± 57.15	0.193 ± 7.8E-04	41.36 ± 0.33

3.2.2. Fourier transform infrared spectroscopy

Fourier transform infrared spectroscopy (FTIR) spectra of CNCs and synthesized polyurethane foams are shown in Figure 5.

All samples showed typical infrared spectra of polyurethane foams. Peaks related to the stretching vibration of N-H (3292 cm^{-1}), C=O (1724 cm^{-1}), C-O (1220 cm^{-1}) groups were identified. The band corresponding to isocyanate group (2270 cm^{-1}) was not observed, which

evidenced that foaming reaction was completed in all cases. Regarding the N-H peak, a shoulder was observed at higher wavemunber in foam nanocomposites when compared to neat foams, attributed to the presence of CNCs (Santamaria-Echart et al., 2016). In the carbonyl stretching region the apparition of a small peak was observed in foam nanocomposites at around (1710 cm^{-1}) which could be related to ordered urethane or free urea. Apart from this, changes in the intensity of bidentate urea (1640 cm^{-1}) were observed. Results suggested that the incorporation of CNCs influenced the microstructure of the foams changing the interactions between urethane and urea containing phases, also observed in other works concerning PU foam CNC nanocomposites (Cordero et al., 2015).

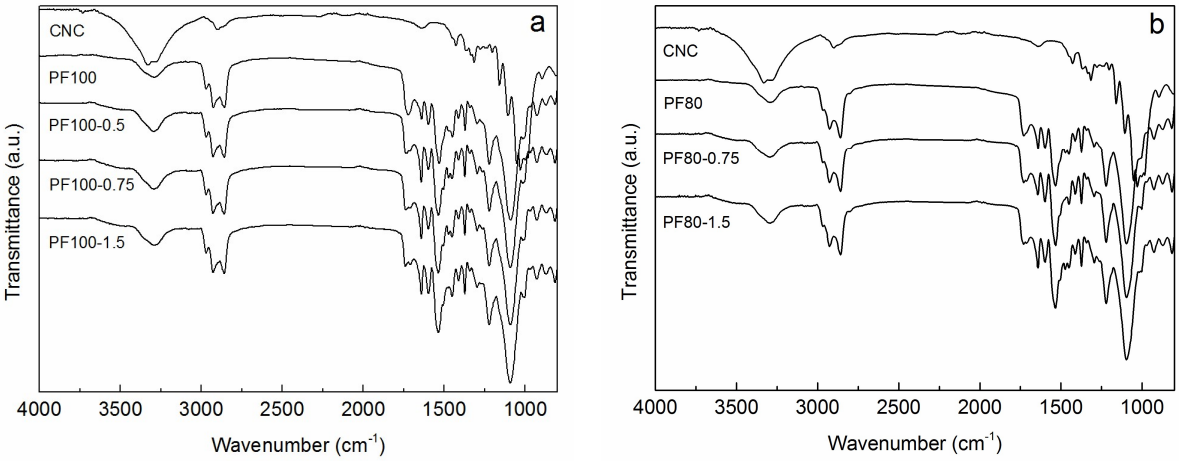

Figure 5. FTIR spectra of (a) PF100 series and (b) PF80 series

3.2.3. Compressive properties

The incorporation of CNCs enhanced the compressive modulus in both PF100 and PF80 series with respect to the neat foam. Increases of 57.1 and 64.8% were obtained for PF100-0.5 and PF80-0.75 samples, respectively. Observing Figure 6a, it was observed that the modulus seemed to reach a plateau above 0.5 CNC wt% in PF100 series, probably due to

some CNC aggregates were formed at high CNC percentages and their reinforcing effect diminished. The big cells observed in SEM images for these foam nanocomposites could also have influenced this behavior. PF80 series showed higher modulus values both for the bare foam and the nanocomposites. Compressive strength values were also improved with CNCs incorporation. Increases of 45.3 and 22% were obtained for PF100-0.5 and PF80-1.5 samples, respectively. PF80 series showed an increasing tendency with CNC incorporation. Compressive strength seemed susceptible to the presence of the aforementioned big cells in PF100 series, as it is shown in Figure 6b. Tien et al. (Tien and Wei, 2001) observed that the enhancement of mechanical properties was a balance between the reinforcing effect of the filler and its effect over polymer morphology. According to these, at low filler contents better dispersions could be obtained and better interactions occurred between CNCs and polymer enhancing mechanical properties. At high filler contents, the obtaining of a fine dispersion is tougher and CNCs affect the polymer morphology to a lower extent. The lower interfacial area between the matrix and the reinforcement hinders the enhancement of mechanical properties. Apart from this, results showed that in foam nanocomposites, the morphology of cellular structure also had considerable influence on the mechanical properties.

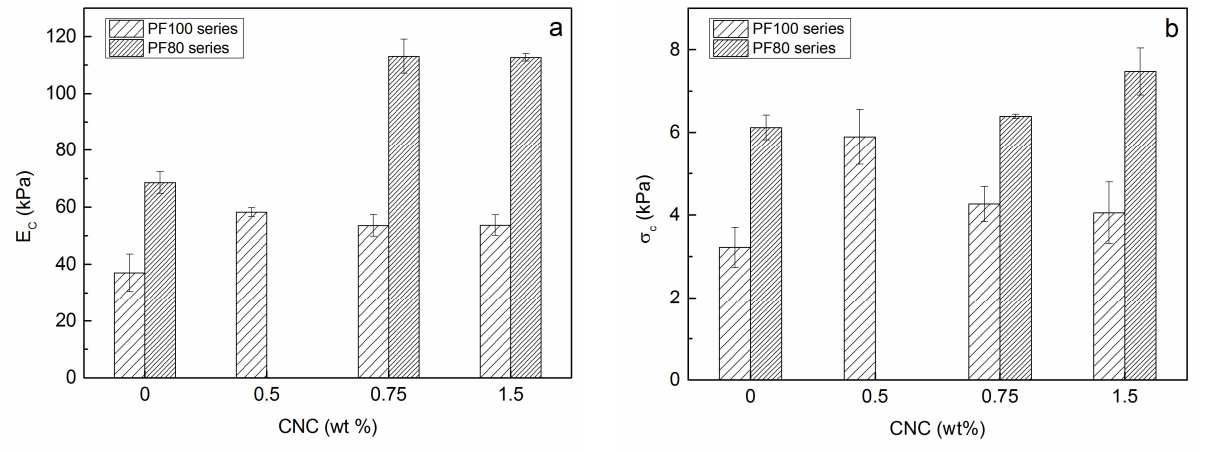

Figure 6. (a) Compressive modulus and (b) compressive strength of neat PU foam and foam nanocomposites

3.2.4. Mechanical hysteresis and resilience

The hysteresis loss during the first compression cycle was calculated and results are summarized in Table 3. The hysteresis curves for PF100 and PF80 series are shown in Figure 7. Hysteresis loss reflects the energy dissipation during cyclic deformation and is characteristic of viscoelastic materials (Alzoubi and Tanbour, 2011; Brinson and Brinson, 2008). It is an important indicator in applications such as bedding to determine the comfort level since it measures the amount of pressure relieving of the material (Alzoubi and Tanbour, 2011). In open cell flexible foams, the amount of hysteresis depends on the viscous flow of contained air and the hysteresis in polymer deformation (Eaves, 2004). Thus, the density and cellular structure together with the polymer morphology are considered important characteristics affecting hysteresis behavior (Malewska et al., 2015). In fact, if specific hysteresis values were calculated, Table 3, it was observed that values correlated quite well with CNC content regardless of density values, confirming that changes in polymer morphology related to CNCs also affected the material behavior.

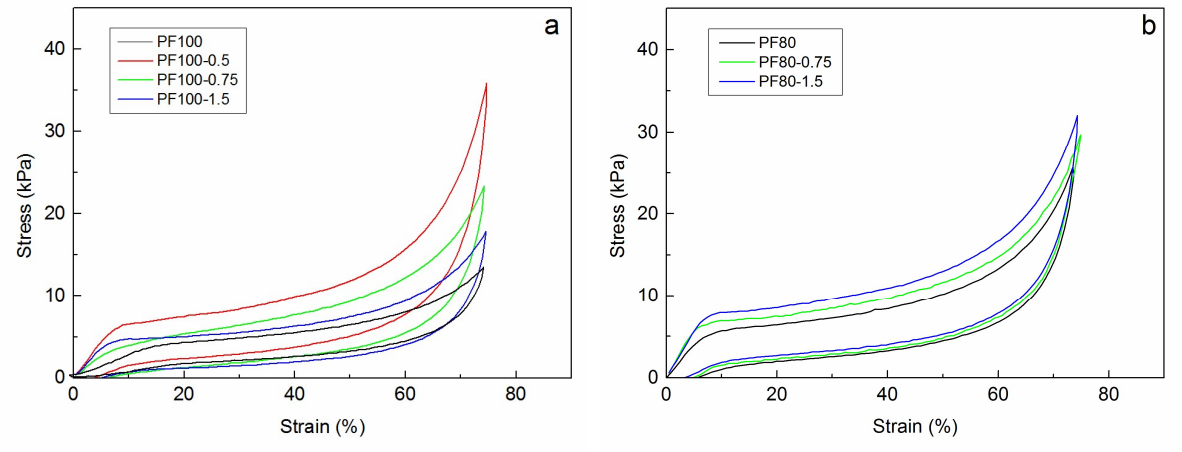

Figure 7. Hysteresis curves of (a) PF100 series and (b) PF80 series.

With difference to hysteresis, resilience measures the capacity to store energy instead of the capacity to disperse energy. As shown in Table 3 and contrary to hysteresis values, resilience decreased in foam nanocomposites in accordance to a more viscoelastic behavior and improved energy absorption properties. Similar behavior was observed in literature regarding polymer foam nanocomposites (Kynard, 2011).

Table 3. Hysteresis and resilience values of analyzed samples.

Sample	Hysteresis (%)	Specific hysteresis (% m^3 kg^{-1})	Resilience (%)
PF100-0	47.40 ± 0.70	1.13	41.7 ± 1.23
PF100-0.5	59.5 ± 1.41	1.44	32.9 ± 0.67
PF100-0.75	57.97 ± 1.19	1.50	37.9 ± 0.47
PF100-1.5	60.86 ± 1.11	1.80	31.97 ± 1.15
PF80-0	49.30 ± 2.96	1.16	39.47 ± 0.75
PF80-0.75	59.3 ± 1.10	1.73	30.6 ± 1.24
PF80-1.5	57.3 ± 1.11	1.39	36.17 ± 1.36

3.2.5. DMA

DMA curves obtained for PF100 and PF80 series in tensile mode are shown in Figure 8a and Figure 8b, respectively.

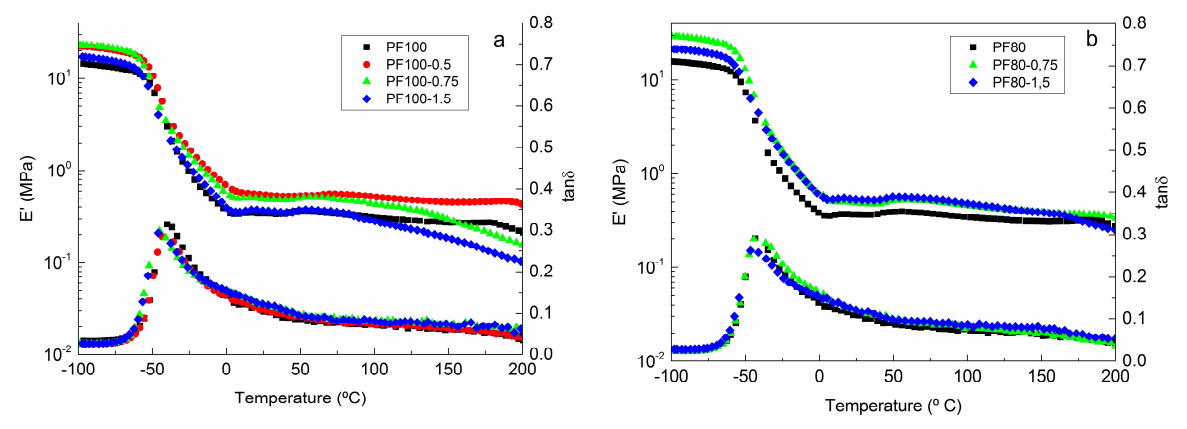

Figure 8. Storage modulus (E') and tanδ curves of (a) PF100 series and (b) PF80 series

The maximum of the tanδ curve was taken as an indication of the glass transition temperature (T_g) of the samples. As it is observed in Figure 8, a general reduction on the T_g values occurred with the incorporation of the CNCs. This could be indicative of the increase of mobility of the soft segments as a result of the interactions occurring between the nanoparticles and the hard segments (Bernal et al., 2012), as FTIR results suggested. Storage modulus values showed higher values with the incorporation of CNCs also in tensile mode, both below the T_g and at room temperature well above the T_g. In general, E' values followed the tendency observed in compressive modulus. Foam nanocomposites with higher CNC contents showed a decrease in thermomechanical stability, reflected as a drop in E' value at temperatures around 100 ºC and 150 ºC for PF100 and PF80 series, respectively. This behavior could be due to the agglomerates of CNC formed at high CNC contents, which act as defects in the stretching direction.

3.2.6. AFM

AFM analysis was performed to observe the influence of matrix composition and CNC content in foam morphology. Results are shown in Figure 9.

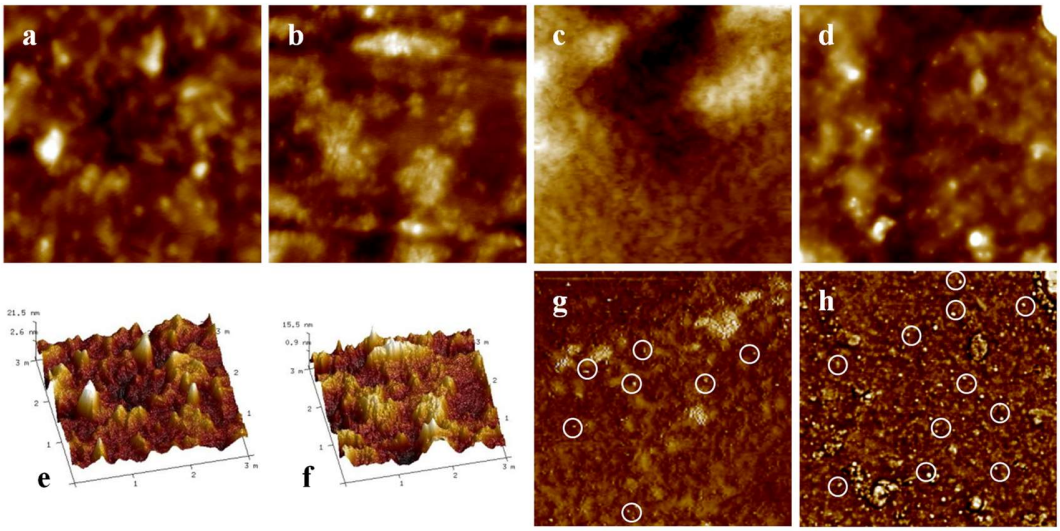

Figure 9. AFM height images of (a) PF100, (b) PF80, (c) PF80-0.75, (d) PF80-1.5, AFM topography images of (e) PF100 (f) PF80 and AFM phase images of (g) PF80-0.75 and (h) PF80-1.5. Circles indicate high phase contrast spots which might be CNCs. All images have a size of 3x3 µm.

Images corresponding to bare PU foams (Figure 9a and Figure 9b) showed similar structures composed by bright and dark regions, as also observed in their corresponding topographic images (Figure 9e and Figure 9f). Bright areas may correspond to rigid ordered urea rich phases in the polyurethane foam (Ugarte et al., 2014). According to this, an increase of hard phases could be observed in PF80 foam. PF80-0.75 sample (Figure 9c) showed a finer

structure compared the bare PF80 foam. According to mechanical testing and DMA results, the improvement of mechanical and thermomechanical behavior observed in PF80-0.75 could be related with the good dispersion of CNC and its impact in foam morphology. Regarding PF80-1.5 sample (Figure 9d), the structure is more similar to the PF80 matrix, possibly due to the poorer dispersion of CNCs. Concerning the phase images of foam nanocomposites (Figure 9g and Figure 9h), dispersed bright spots (indicated with white circles) were observed in the polyurethane matrix, which may be the CNCs. A higher quantity of them was observed in PF80-1.5 sample corresponding to its higher CNC quantity. For the verification of the presence of CNCs in the foam walls and struts, nano-FTIR and s-SNOM analysis were performed.

3.2.7. Nano-FTIR spectroscopy and s-SNOM imaging.

Nano-FTIR spectroscopy and IR s-SNOM imaging were applied to verify the distribution of CNCs in PF80-1.5 sample. To that end, firstly a nano-FTIR spectrum of a pure CNC sample was recorded, shown in Figure 10a. Significant peaks around 1100 cm^{-1} were observed, in good agreement with the FTIR spectrum of Fig. 5. Frequencies where CNC absorption is absent (929 cm^{-1}) and strong (1050 cm^{-1}) were determined from the spectrum. PF800-1.5 sample was subsequently imaged by s-SNOM at these two frequencies (IR s-SNOM phase images shown in Figure 10b). At 1050 cm^{-1} a homogenous distribution of small spots exhibiting strong infrared phase contrast was observed, which are not seen at 929 cm^{-1}. Based on the nano-FTIR phase spectrum of pure CNC, it can be concluded that the spots of strong phase contrast at 1050 cm^{-1} reveal the CNC particles. The very few spots of strong phase contrast at 929 cm^{-1} are attributed to sample contaminations. Further, comparison with the AFM phase image (Figure 10c, right) shows that spots of strong infrared contrast coincide

with spots of strong AFM contrast (see white circles in Figures 10b and 10c). Although the images in Figure 9h and Figure 10c were taken in different locations on the sample, the distribution of bright spots marked in circles is similar in both samples. Taking this into account, the bright spots on Figure 9h might also correspond to the dispersed CNCs.

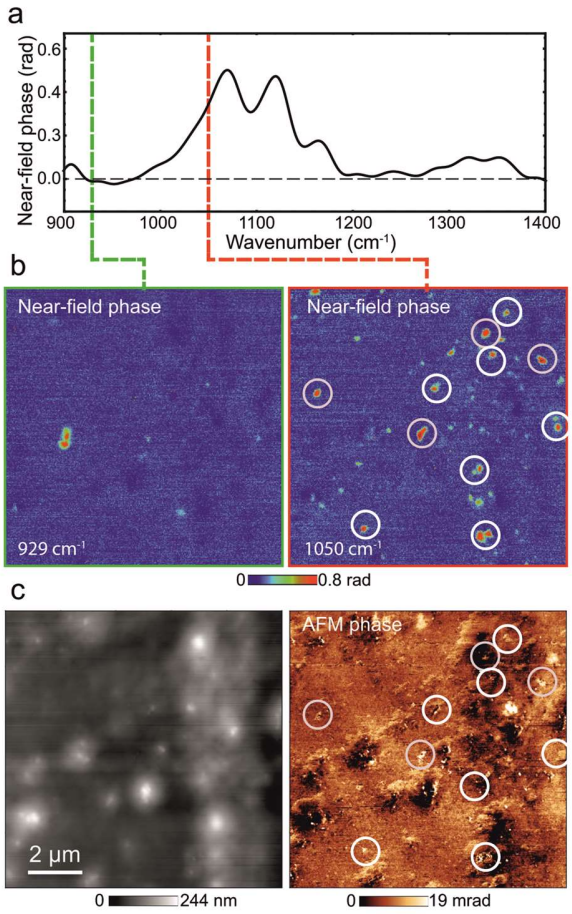

Figure 10. (a) nano-FTIR phase spectrum of a pure CNC sample. (b) Infrared s-SNOM phase images of a foam cross-section. The two images show the same sample area at 929 cm^{-1} and 1050 cm^{-1}. (c) AFM topography and phase images, taken simultaneously with the infrared image at 929 cm^{-1} (Fig. 10b). The white circles in b) and c) highlight particles showing both strong phase contrast and infrared contrast at 1050 cm^{-1}.

4. CONCLUSIONS

CNCs of rod-like shape were successfully isolated by acid hydrolysis from microcrystalline cellulose and incorporated directly in aqueous suspension to flexible polyurethane foam synthesis. Changes due to the presence of CNCs were observed at different levels regarding micro/nanostructure, foam morphology and final properties. SEM images revealed changes in the foam cell morphology when CNCs were added. Compressive mechanical properties were enhanced with CNC incorporation, especially in formulations with low CNC contents. In fact, increases up to 57.1 and 64.8% were obtained for PF100-0.5 and PF80-0.75 samples respectively regarding the compressive modulus and increases up to 45.3 and 22% were obtained for PF100-0.5 and PF80-1.5 samples respectively regarding the compressive strength. The level of reinforcement seemed to be dependent on obtaining of a good dispersion of CNCs and in the foam cell morphology. The energy absorption capacity and viscoelastic behavior of foams increased when CNCs were incorporated. DMA analysis showed an increase on storage modulus values in comparison with neat foams. Damping factor (tanδ) curves suggested that CNCs influenced the interactions between hard and soft segments modifying polymer micro/nanostructure. AFM images revealed that CNCs interfered in the bare polymer foam micro/nanostructure, especially in those nanocomposites where mechanical and thermomechanical properties improved the most. By means of nano-FTIR technique bright spots observed in AFM images were identified as CNCs in the polyurethane matrix. An increase of bright spots according to CNC percentage was observed in AFM phase images.

Acknowledgements

Financial support from the Basque Government in the frame of Grupos Consolidados (IT-776-13) and Department of Industry (ETORTEK 2014-CORROPTO project) together with Spanish Ministry of Economy and Competitiveness (MAT2013-43076-R and MAT2015-65525-R) and European Union-FP7-PIRSES-GA-2012-BIOPURFIL program are gratefully acknowledged. Additionally, the L.U. thanks the University of the Basque Country (UPV/EHU) for funding this work (PIFUPV047/2011). The authors also thank for technical and human support provided by SGIker of UPV/EHU and European funding (ERDF and ESF).

References

Alavi Nikje, M.M., Tamaddoni Moghaddam, S., Noruzian, M., Farahmand Nejad, M.A., Shabani, K., Haghshenas, M., Shakhesi, S., 2014. Preparation and characterization of flexible polyurethane foam nanocomposites reinforced by magnetic core-shell Fe3O4@APTS nanoparticles. Colloid Polym. Sci. 292, 627–633. doi:10.1007/s00396-013-3099-2

Alzoubi, M.F., Tanbour, E.Y., 2011. Compression and hystheresis curves of nonlinear polyurethane foams under different densities, strain rates and different environmental conditions, in: Proceedings of the ASME 2011 International Mechanical Engineering Congress & Exposition IMECE2011. pp. 1–9. doi:10.1115/IMECE2011-62290

Beck, S., Bouchard, J., Berry, R., 2012. Dispersibility in water of dried nanocrystalline cellulose. Biomacromolecules 13, 1486–1494. doi:10.1021/bm300191k

Bernal, M.M., Lopez-Manchado, M.A., Verdejo, R., 2011. In situ foaming evolution of flexible polyurethane foam nanocomposites. Macromol. Chem. Phys. 212, 971–979.

doi:10.1002/macp.201000748

Bernal, M.M., Molenberg, I., Estravis, S., Rodriguez-Perez, M.A., Huynen, I., Lopez-Manchado, M.A., Verdejo, R., 2012. Comparing the effect of carbon-based nanofillers on the physical properties of flexible polyurethane foams. J. Mater. Sci. 47, 5673–5679. doi:10.1007/s10853-012-6331-4

Brinson, H.F., Brinson, L.C., 2008. Polymer engineering science and viscoelasticity. An introduction. Springer, New York, NY.

Cordero, A.I., Amalvy, J.I., Fortunati, E., Kenny, J.M., Chiacchiarelli, L.M., 2015. The role of nanocrystalline cellulose on the microstructure of foamed castor-oil polyurethane nanocomposites. Carbohydr. Polym. 134, 110–118. doi:10.1016/j.carbpol.2015.07.077

De Oliveira Patricio, P.S., Pereira, I.M., Da Silva, N.C.F., Ayres, E., Pereira, F.V., Oréfice, R.L., 2013. Tailoring the morphology and properties of waterborne polyurethanes by the procedure of cellulose nanocrystal incorporation. Eur. Polym. J. 49, 3761–3769. doi:10.1016/j.eurpolymj.2013.08.006

Dong, X.M., Gray, D.G., 1997. Effect of counterions on ordered phase formation in suspensions of charged rodlike cellulose crystallites. Langmuir 13, 2404–2409. doi:10.1021/la960724h

Dong, X.M., Revol, J.-F., Gray, D.G., 1998. Effect of microcrystallite preparation conditions on the formation of colloid crystals of cellulose. Water 5, 19–32. doi:10.1023/A:1009260511939

Eaves, D., 2004. Handbook of polymer foams. Rapra Technology, Shrewsbury, UK.

Espinosa, S.C., Kuhnt, T., Foster, E.J., Weder, C., 2013. Isolation of thermally stable cellulose nanocrystals by phosphoric acid hydrolysis. Biomacromolecules 14, 1–27. doi:dx.doi.org/10.1021/bm400219u

Govyadinov, A.A., Amenabar, I., Huth, F., Carney, P.S., Hillenbrand, R., 2013. Quantitative measurement of local infrared absorption and dielectric function with tip-enhanced near-field microscopy. J. Phys. Chem. Lett. 4, 1526–1531. doi:10.1021/jz400453r

Govyadinov, A.A., Mastel, S., Golmar, F., Chuvilin, A., Carney, P.S., 2014. Recovery of permittivity and depth from near-field data as a step toward infrared nanotomography. ACS Nano 8, 6911–6921. doi:10.1021/nn5016314

Hussain, F., Hojjati, M., Okamoto, M., 2006. Review article: polymer-matrix nanocomposites, processing, manufacturing, and application: an overview. J. Compos. Mater. 40, 1511–1575. doi:10.1177/0021998306067321

Huth, F., Govyadinov, A., Amarie, S., Nuansing, W., Keilmann, F., Hillenbrand, R., 2012. Nano-FTIR absorption spectroscopy of molecular fingerprints at 20 nm spatial resolution. Nano Lett. 12, 3979–3978. doi:10.1021/nl301159v

Huth, F., Schnell, M., Wittborn, J., Ocelic, N., Hillenbrand, R., 2011. Infrared-spectroscopic nanoimaging with a thermal source. Nat. Mat. 10, 352–356. doi:10.1038/nmat3006

Jonoobi, M., Oladi, R., Davoudpour, Y., Oksman, K., Dufresne, A., Hamzeh, Y., Davoodi, R., 2015. Different preparation methods and properties of nanostructured cellulose from various natural resources and residues: a review. Cellulose 22, 935–969. doi:10.1007/s10570-015-0551-0

Keilmann, F., Hillenbrand, R., 2009. Nano-optics and near-field optical microscopy. Artech House, Boston/London.

Khoshkava, V., Kamal, M.R., 2014. Effect of drying conditions on cellulose nanocrystal (CNC) agglomerate porosity and dispersibility in polymer nanocomposites. Powder Technol. 261, 288–298. doi:10.1016/j.powtec.2014.04.016

Klemm, D., Heublein, B., Fink, H.P., Bohn, A., 2005. Cellulose: Fascinating biopolymer and

sustainable raw material. Angew. Chemie - Int. Ed. 44, 3358–3393. doi:10.1002/anie.200460587

Kvien, I., Tanem, B.S., Oksman, K., 2005. Characterization of cellulose whiskers and their nanocomposites by atomic force and electron microscopy. Biomacromolecules 6, 3160–3165. doi:10.1021/bm050479t

Kynard, K., 2011. PMMA carbon nanotube nanocomposite foams for energy dissipation. Ph. D. Dissertation. Florida State University, Tallahassee, FL.

Lan, Q., Haugstad, G., 2011. Characterization of polymer morphology in polyurethane foams using atomic force microscopy. J. Appl. Polym. Sci. 121, 2644–2651. doi:10.1002/app.34005

Malewska, E., Bak, S., Prociak, A., 2015. Effect of different concentration of rapeseed-oil-based polyol and water on structure and mechanical properties of flexible polyurethane foams. J. Appl. Polym. Sci. 132, 42372 (1-11). doi:10.1002/app.36500

Mariano, M., El Kissi, N., Dufresne, A., 2014. Cellulose nanocrystals and related nanocomposites: Review of some properties and challenges. J. Polym. Sci. Part B Polym. Phys. 52, 791–806. doi:10.1002/polb.23490

Mastel, S., Govyadinov, A.A., de Oliveira, T.V.A.G., Amenabar, I., Hillenbrand, R., 2015. Nanoscale-resolved chemical identification of thin organic films using infrared near-field spectroscopy and standard Fourier transform infrared references. Appl. Phys. Lett. 106, 023113/1-023113/5. doi:10.1063/1.4905507

Mittal, V., 2010. Optimization of Polymer Nanocomposite Properties. Willey, Weinheim, Germany.

Mosiewicki, M.A., Rojek, P., Michalowski, S., Aranguren, M.I., Prociak, A., 2015. Rapeseed oil-based polyurethane foams modified with glycerol and cellulose micro/nanocrystals.

J. Appl. Polym. Sci. 132, 9–12. doi:10.1002/app.41602

Petrovic, Z., 2008. Polyurethanes from vegetable oils. Polym. Rev. 48, 109–155. doi:10.1080/15583720701834224

Ramôa, S.D.A.S., Barra, G.M.O., Oliveira, R.V.B., De Oliveira, M.G., Cossa, M., Soares, B.G., 2013. Electrical, rheological and electromagnetic interference shielding properties of thermoplastic polyurethane/carbon nanotube composites. Polym. Int. 62, 1477–1484. doi:10.1002/pi.4446

Rueda, L., Saralegi, A., Fernández-d'Arlas, B., Zhou, Q., Alonso-Varona, A., Berglund, L.A., Mondragon, I., Corcuera, M.A., Eceiza, A., 2013a. In situ polymerization and characterization of elastomeric polyurethane-cellulose nanocrystal nanocomposites. Cell response evaluation. Cellulose 20, 1819–1828. doi:10.1007/s10570-013-9960-0

Rueda, L., Saralegui, A., Fernández d'Arlas, B., Zhou, Q., Berglund, L.A., Corcuera, M.A., Mondragon, I., Eceiza, A., 2013b. Cellulose nanocrystals/polyurethane nanocomposites. Study from the viewpoint of microphase separated structure. Carbohydr. Polym. 92, 751–757. doi:10.1016/j.carbpol.2012.09.093

Santamaria-Echart, A., Ugarte, L., Arbelaiz, A., Gabilondo, N., Corcuera, M.A., Eceiza, A., 2016. Two different incorporation routes of cellulose nanocrystals in waterborne polyurethane nanocomposites. Eur. Polym. J. 76, 99–109. doi:10.1016/j.eurpolymj.2016.01.035

Saralegi, A., Gonzalez, M.L., Valea, A., Eceiza, A., Corcuera, M.A., 2014. The role of cellulose nanocrystals in the improvement of the shape-memory properties of castor oil-based segmented thermoplastic polyurethanes. Compos. Sci. Technol. 92, 27–33. doi:10.1016/j.compscitech.2013.12.001

Tien, Y.I., Wei, K.H., 2001. Hydrogen bonding and mechanical properties in segmented

montmorillonite/polyurethane nanocomposites of different hard segment ratios. Polymer (Guildf). 42, 3213–3221. doi:10.1016/S0032-3861(00)00729-1

Ugarte, L., Gómez-Fernández, S., Peña-Rodríguez, C., Prociak, A., Corcuera, M.A., Eceiza, A., 2015. Tailoring mechanical properties of rigid polyurethane foams by sorbitol and corn derived biopolyol mixtures. ACS Sustain. Chem. Eng. 3, 3382–3387. doi:10.1021/acssuschemeng.5b01094

Ugarte, L., Saralegi, A., Fernández, R., Martín, L., Corcuera, M.A., Eceiza, A., 2014. Flexible polyurethane foams based on 100% renewably sourced polyols. Ind. Crops Prod. 62, 545–551. doi:10.1016/j.indcrop.2014.09.028

Valentini, M., Piana, F., Pionteck, J., Lamastra, F.R., Nanni, F., 2015. Electromagnetic properties and performance of exfoliated graphite (EG) – Thermoplastic polyurethane (TPU) nanocomposites at microwaves. Compos. Sci. Technol. 114, 26–33. doi:10.1016/j.compscitech.2015.03.006

Viet, D., Beck-Candanedo, S., Gray, D.G., 2007. Dispersion of cellulose nanocrystals in polar organic solvents. Cellulose 14, 109–113. doi:10.1007/s10570-006-9093-9

Williams, C.K., Hillmyer, M.A., 2016. Polymers from renewable resources : a perspective for a special issue of polymer reviews. Polym. Rev. 48, 3724 (1-10). doi:10.1080/15583720701834133

Zhang, C., Madbouly, S.A., Kessler, M.R., 2015. Biobased polyurethanes prepared from different vegetable oils. ACS Appl. Mater. Interfaces 7, 1226–1233. doi:10.1021/am5071333